APPLICATION OF DISPLACED PING IMAGING AUTOFOCUS ALGORITHM TO SAS TRIALS DATA

JE Coote Frazer-Nash Consultancy, UK
RS Aldred Frazer-Nash Consultancy, UK

1 INTRODUCTION

The preservation of maritime freedom of manoeuvre is a strategic priority for the Royal Navy. In order to achieve it over the coming years, Autonomous Underwater Vehicles (AUVs) are anticipated to be a key element of future mine countermeasures (MCM) capability. MCM has particular relevance to shallow waters, as many threats are associated with coastal areas, ports and inland waterways. The ability to detect and classify mine-like objects benefits significantly from the ability to obtain high-resolution sonar imagery via techniques including high-frequency active synthetic aperture sonar (SAS).

SAS requires that the relative positions of virtual transducers in a synthetic array are known to sub-wavelength accuracy in order to allow coherent integration of data from multiple pings to form a SAS image. For AUVs, this translates into a requirement to know the rigid-body motion between transmitted pings to within a fraction of a wavelength referred to as the 'micronavigation' problem[1]. Image resolution improves with operating frequency, thus higher-resolution sonars impose tighter requirements; as an example, a 300kHz sonar has wavelength ~5mm. Current onboard navigation systems are typically not sufficiently accurate to meet these tolerances over useful distances. Micronavigation may instead (or in conjunction) be achieved by deriving information about relative positioning from the echo data. The Displaced Phase Centre Antenna (DPCA) technique is one common approach.

DPCA (e.g. [2]) involves the notional creation of a set of bistatic pairings between transmitter elements and receiver elements. An approximation is then made that the returns measured at any given receiving element is equivalent to those that would be recorded by a collocated transmit/receive element situated at the phase centre (i.e. median position) of the given bistatic pair. If the sonar array is aligned with the direction of travel, there can be a degree of overlap between one phase centre at the time of one transmitted ping and a different phase centre at the time of a subsequent ping (Figure 1). Under the approximation, the signal measured at the two overlapping phase centres is the same, and the cross-correlation shows a single strong peak at zero lag. If one of the paired phase centres is displaced laterally, this is observable in the cross-correlation as a shift of the peak to a non-zero lag. The ping-to-ping sway displacement (Figure 1) may therefore be inferred by observing the position of the cross-correlation peak. This may be repeated for a number of phase centre pairings along the sonar array; as the array is of known geometry, additional constraints can be applied to the inferred displacements (e.g. enforced collinearity of array elements) to further improve the quality of the measurements and obtain an estimate of relative yaw. Variation of forward velocity along the longitudinal body axis (surge) may be estimated by determining the optimal pairing of phase centres between each transmitted ping and the next, although it is likely that better estimates may be obtained via inertial navigation aided by a Doppler velocity log. Variation of depth (heave) and roll may also be relevant but generally present fewer difficulties in this context.

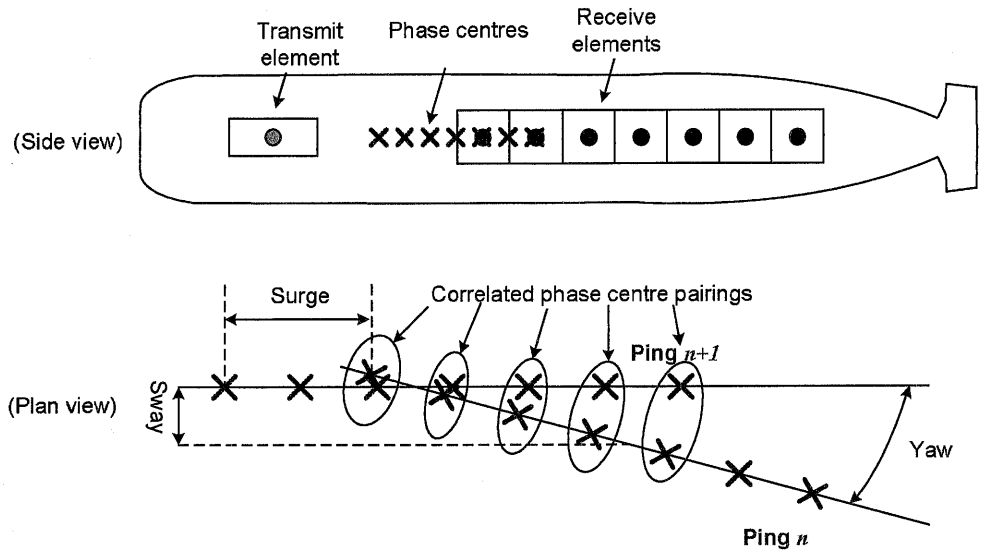

Figure 1: Schematic showing pairing of phase centres of successive pings as part of DPCA.

DPCA relies on the existence of a single clear peak in the cross-correlation between the recorded signals associated with paired phase centres. This may not always be the case. Multiple peaks can result from a target scene with periodic reflectivity (e.g. rippled seabed) or strong reflections of echoes (e.g. multipath reflections from seabed and/or sea surface). Alternatively, there may be uniformly poor correlation where large numbers of diffuse point scatterers exist (e.g. surf, particulates) or if the target scene is nonstationary. DPCA may then be rendered ineffective as an unambiguous correlation peak may no longer be present, precluding effective SAS post-processing.

The current study seeks to investigate whether an alternative technique, Displaced Ping Imaging Autofocus[9] (DPIA), affords effective micronavigation with respect to a particular set of trials data where previously DPCA has not worked effectively. While DPCA uses raw measurements from individual sonar array elements and then averages the estimation across multiple elements, DPIA (described in Section 2) is an image-based approach that uses the full information over all elements. It might therefore be reasonably expected that DPIA can tolerate a lower signal-to-noise ratio than DPCA, provided that the imaged scene is not devoid of features. The authors are not aware of any published results relating to the application of DPIA to trials data. DPIA has been implemented and applied to the data; the remainder of this paper describes the methods and outcomes.

2 THE DISPLACED PING IMAGING AUTOFOCUS (DPIA) TECHNIQUE

DPCA imposes a constraint on spatial sampling and hence on mapping rate. Displaced Ping Imaging Autofocus (DPIA) was introduced in [9] and was motivated by the desire to avoid this constraint. There was potential for DPIA to exhibit improved robustness over DPCA in the presence of multipath signals, leading to its selection as the subject of the present study.

In DPIA, real aperture images are produced for each ping in isolation using the received signal at all elements of the line array. The two images associated with any successive pair of pings may be co-registered, assuming sufficient overlap and consistency. The translation and rotation required to map one image to the other may then be used to infer the relative sway and yaw of the sonar array

for each ping pair. (For the case studied, the relative surge is better estimated with reference to the inertial navigation system and Doppler velocity log). This process is depicted in Figure 2.

Compared with DPCA, DPIA is released from the requirement for overlapping phase centres, allowing the sonar to travel a greater distance forwards between pings. This is replaced by a requirement that individual array elements have sensitivity over sufficiently wide angles to enable the real aperture images from successive pings to overlap for the ranges of interest. DPIA further requires a sufficient number of array elements to form a low-resolution image from a single ping.

A numerical study[9] previously demonstrated DPIA on synthetic data, although the parameters differ from those in the current study. The study presented various DPIA implementation options, and the main elements of approach taken in the current work are described in the following subsections.

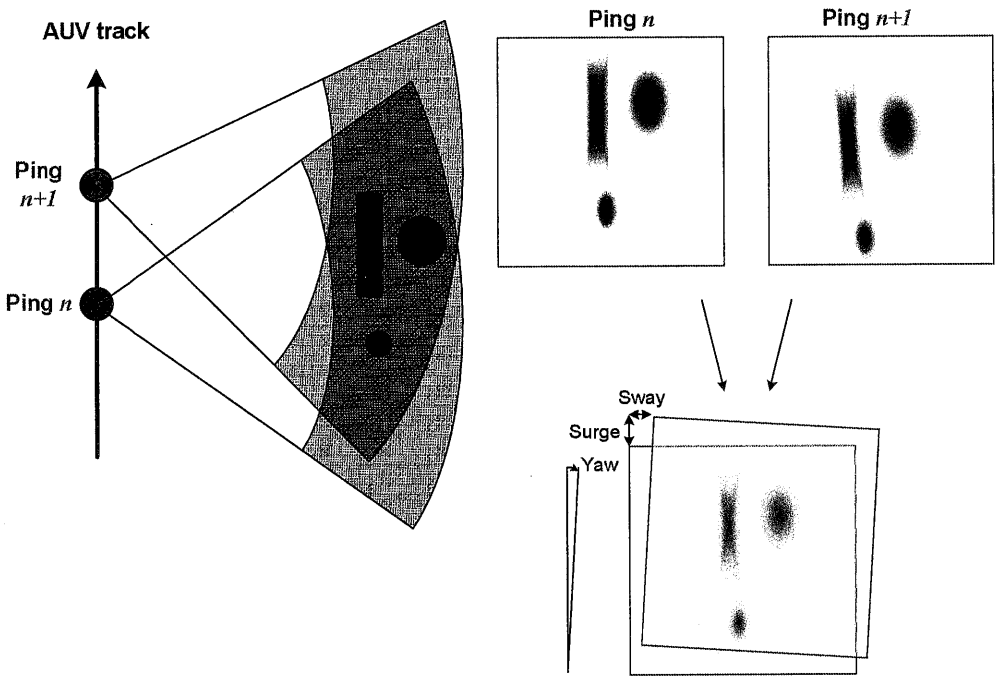

Figure 2: Schematic depiction of DPIA algorithm.

2.1 Single-ping image reconstruction

In order to generate real aperture images from single pings for DPIA, images were generated from data relating to single pings using a time-domain backprojection approach. This consisted of an implementation of Equation 1 in MATLAB over multiple processors. Cubic interpolation was used to define the value of the replica signal at non-integer fractions of the sample time interval.

$$\hat{ff}_p(x,y) = \iint ss_p(t,d) \cdot \wp\left(t - \frac{1}{c}\left[\sqrt{x^2+(y-y_{Tx})^2} + \sqrt{x^2+(y-d)^2}\right]\right) dt \cdot dd \qquad (1)$$

where

$\hat{ff}_p(x,y)$ is the image reconstruction at distance x abeam and distance y up-track of the phase centre of the receive array;

$ss_p(t,d)$ is the complex baseband value of the recorded echo at time t for the receive array element at distance d uptrack of the phase centre, following element-specific calibration;

$\wp(t)$ is the complex value of the replica of the transmitted chirp at time t;

c is the local speed of sound in water (~1500m/s although more accurate measurements are continually taken while echo data are acquired);
y_{Tx} is the up-track offset of the transmit array phase centre relative to that of the receive array.

Equation 1 results in an exact image reconstruction as desired by the current study, assuming omnidirectional receive element sensitivity. A further investigation considered the inclusion of an additional term to model the directional sensitivity function of individual array elements but the effect was deemed marginal over small angles of azimuth and not justified by the increased computational overhead. Alternative reconstruction algorithms were considered in the interests of significantly accelerated computation (e.g. Equations 15 & 16 in the original paper[9]) however these make simplifying assumptions that are not applicable to the current scenario. Other reconstruction algorithms (Range-Doppler, Wavenumber, Chirp-Scaling) are described elsewhere[10].

The resolution of a single-ping image is a function of the size of the real aperture and the wavelength of transmission:

$$\theta_{3dB} \approx 1.22\alpha\frac{\lambda}{l} \quad (2)$$

$$\partial y_{3dB} = r\theta_{3dB} \quad (3)$$

$$\partial r_{3dB} = \frac{c}{2B} \quad (4)$$

where
θ_{3dB} is the 3dB Rayleigh resolution (broadside);
∂y_{3dB} and ∂r_{3dB} are the 3dB resolutions in the along-track and range directions respectively;
λ and l are wavelength and aperture length respectively;
r is cross-track range;
α is a coefficient to account for any widening of the main lobe due to array shading;
B is the signal bandwidth.

Within the present study, this would predict that the maximum achievable resolutions in the range and along-track directions are ~12.5mm and ~203mm at an indicative range of 40m.

2.2 Image co-registration

Image co-registration is the process of determining the relative transformation that may be applied to one image in order to achieve optimal alignment with a second image. By co-registering images from adjacent pings, the goal is to determine the relative displacement of the sonar platform, thereby enabling coherent SAS post-processing in situations where the DPCA algorithm does not perform sufficiently well.

The present study used commercially-available algorithms within the MATLAB Image Processing Toolbox in preference to implementing the co-registration algorithm suggested[9] for reasons of expediency. Optimality is assessed via an intensity-based correlation criterion; this considers the absolute value of the complex-valued image pixels to represent intensity, consistent with the original paper[9]. The approach is interpolative, allowing significantly sub-pixel accuracies to be obtained as necessary for coherent processing across multiple pings. The co-registration proceeds in several hierarchical stages. The images are initially downsampled to a low resolution and then co-registered. The resolution is then increased and the optimisation is repeated in stages until full resolution and optimality is reached. A range of user parameters allow algorithm fine-tuning depending on the desired balance between efficiency and exactness. Tests of these algorithms on sample SAS imagery (high-resolution) confirmed their ability to successfully co-register translated instances of the same image for typical yaw, sway and surge values, with an example shown in Figure 3 / Figure 4.

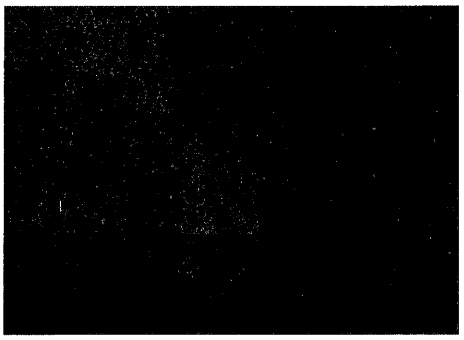

Figure 3: Overlay of original image (green) and transformed image (purple), before co-registration.

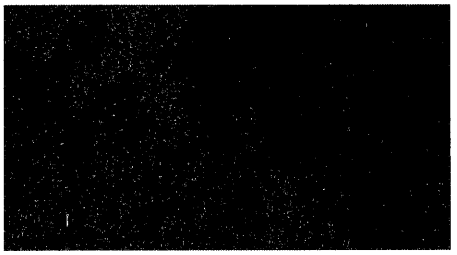

Figure 4: Overlay of the two images after co-registration.

3 TRIALS DATA

The trials data used within this study were provided by NATO Centre for Maritime Research and Experimentation (CMRE) and acquired by the MUSCLE platform (Minehunting UUV for Shallow-water Covert Littoral Expeditions)[4,5]. MUSCLE was developed by Thales Underwater Systems to a high specification as part of a research program set up by NATO Undersea Research Centre (now CMRE) in 1998 with further development ongoing[6].

3.1 The MUSCLE platform

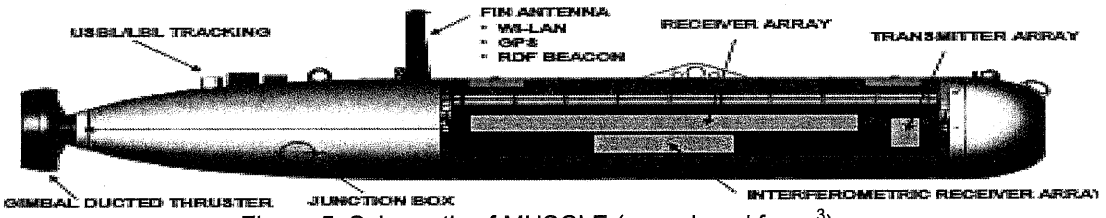

Figure 5: Schematic of MUSCLE (reproduced from [3]).

The MUSCLE sonar consists of a vertical transmit array (to allow angular selectivity for reducing seabed and sea surface multipath echoes) and a 36-element horizontal line array on each side. Each array element has physical width of 33.3mm and horizontal null-to-null beamwidth of 14°. The main receiver horizontal line array is composed of an upper and a lower array (not shown), with only the lower array employed for the work described in this paper. A schematic is shown in Figure 5.

Additional 12-element line arrays are also present beneath the main receiver array on each side, although the data from these are not used in the current study.

MUSCLE also acquires data from other onboard systems, yielding measurements of latitude, longitude, Doppler velocity log, depth, and altitude.

3.2 MUSCLE trials data

As part of the MARES 2008 programme, the MUSCLE platform acquired trials data off the island of Elba at two sites, Punta del Nasuto and Biodola Bay. The quality of the resulting SAS imagery was generally high, with images of a Roman shipwreck at Punta del Nasuto attracting press interest. However, one of the runs at Biodola employed a measurement mode that was suboptimal relative to device capability, causing some failure with the DPCA stage of the SAS processing. MUSCLE

usually employs a multipath mitigation scheme[7] in which two line arrays are available with a 4° difference in depression angle; the signal-to-noise ratio is improved by selecting which array to use for any given echo range. In this instance, the multipath mitigation scheme was not employed, with only the lower row of array elements used (3dB vertical beamwidth of 14°) without any switchover. The transmit beam steering angle was smaller than usual at 12°, and it was operating on the limit of shallow/very shallow water conditions (12m average water depth), for which it was not designed. At the target range, the angle of arrival of the direct seabed return was close to that of the multipath return via a specular reflection from the sea surface and seabed. Without the multipath mitigation scheme, angular selectivity in the vertical plane was reduced, and the reduced signal-to-noise resulted in weak correlations between recorded echoes at phase centres within the DPCA scheme.

Figure 6: Satellite image showing MUSCLE Biodola Bay trial tracks and location of the water-filled cylinder ('WFCyllinder')[8].

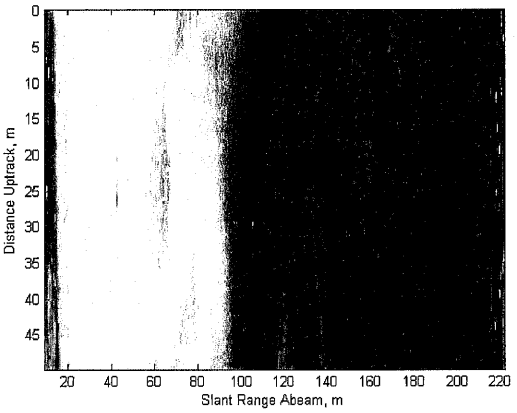

Figure 7: Sidescan sonar image formed from 100 individual pings.

The data considered are taken from a run heading approximately North-Northeast, shown as a green line in Figure 6. This involves passing a 2m-long steel water-filled cylinder on the starboard side tethered to the sea floor at a lateral track offset of ~40m. The data consist of echoes recorded from 100 pings at a forward velocity of ~1.5m/s and a pulse repetition frequency of ~3Hz. Each ping has duration 10ms, centre frequency 300kHz, and consists of a linear frequency modulated chirp with bandwidth 60kHz. The phase centre of the transmit array is located ~0.7m uptrack of the receive array phase centre.

Echoes were measured at each of the 36 array elements at a sampling frequency of 300kHz, digitally down-converted to complex baseband values with a sampling frequency of 75kHz, and phase calibrations applied, yielding the dataset available to the current study.

Figure 7 shows a sidescan image of the surveyed scene. Each row of pixels represents the absolute values of match-filtered data from a single ping beamformed abeam at 40m. The water-filled cylinder is evident at a slant range of ~40m, at a distance of ~25m along the displayed track.

4 APPLICATION OF DPIA TO TRIALS DATA

4.1 Image reconstruction

The recorded echo data from 100 MUSCLE trial pings were processed to generate real-aperture images in each case. Figure 8 to Figure 12 illustrate the process for two particular transmitted pings, one abeam the cylinder (ping 730) and one away from it (ping 690), representing scenarios

with/without strong features respectively. These figures qualitatively highlight the relative detail available in the sway direction and the limited ability to resolve the image azimuthally.

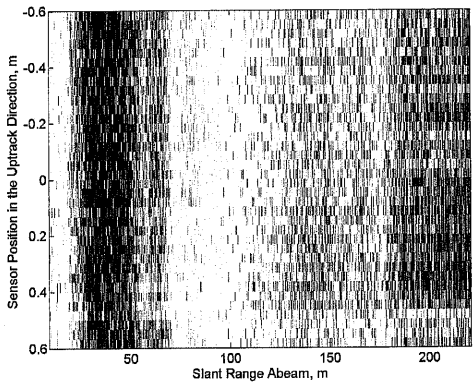

Figure 8: Echo data by sensor for ping 690 (no cylinder present).

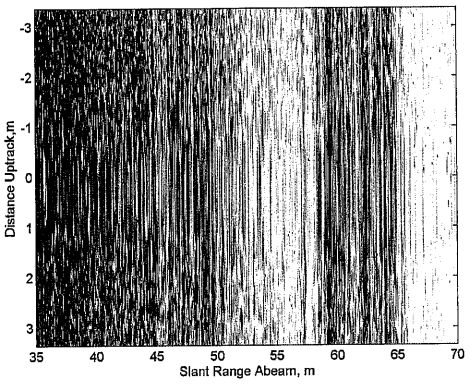

Figure 9: Processed real-aperture image for ping 690 (no cylinder present).

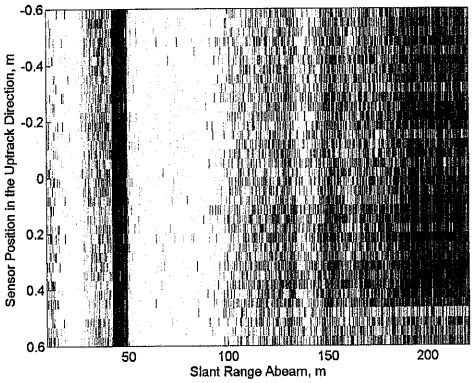

Figure 10: Echo data by sensor for ping 730 (with cylinder).

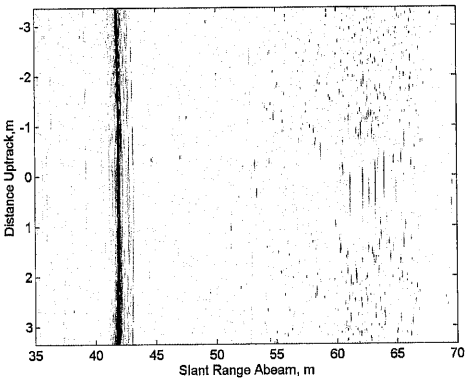

Figure 11: Processed real-aperture image for ping 730 (with cylinder).

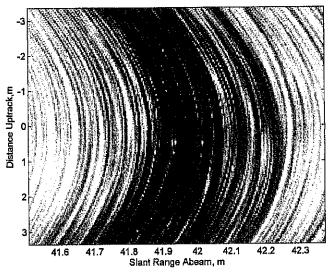

Figure 12: Figure 11, x-axis expanded.

4.2 Co-registration of real-aperture imagery from trials data

While many ping pairs were considered in the current study, pings 690/691 and pings 730/731 will be presented to illustrate all the findings of this study. These figures in this section are to be interpreted qualitatively; the x-axis shows slant range, the y-axis shows distance uptrack, and absolute magnitude is shown as colour intensity (red or blue, depending on whether the image is respectively the first or second in the ping pair).

Real-aperture images from ping 690, 691, and the co-registered pair of pings, are shown respectively in Figure 13, Figure 14 and Figure 15. The images are not feature-rich or particularly similar in detail between pings and it is not apparent that the co-registration could be optimised any further. Real-aperture images from ping 730, 731, and the co-registered pair of pings, are shown

respectively in Figure 16, Figure 17 & Figure 18, with the x-axis greatly expanded to show the detail of the cylinder return.

Figure 13: Real-aperture image reconstruction of ping 690 (absolute value shown as red intensity).

Figure 14: Real-aperture image reconstruction of ping 691 (absolute value shown as blue intensity).

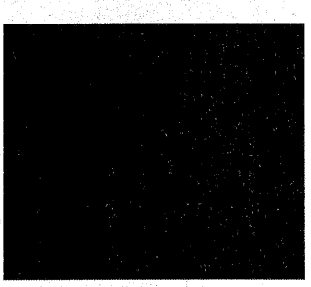

Figure 15: Co-registered image pair for pings 690/691.

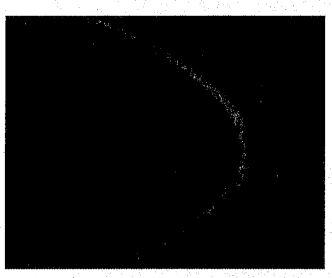

Figure 16: Zoomed real-aperture image reconstruction of ping 730 (absolute value shown as red intensity).

Figure 17: Zoomed real-aperture image reconstruction of ping 731 (absolute value shown as blue intensity).

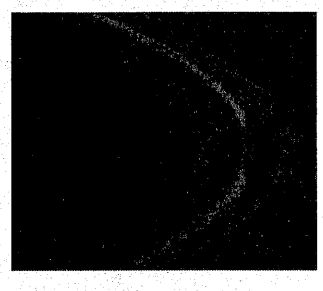

Figure 18: Co-registered image pair for pings 730/731 (zoomed detail).

The point of greatest intensity in Figure 16 is higher up on the main arc compared to Figure 17, reflecting the up-track progress of MUSCLE between the two pings. The co-registration has aligned the arc features as well as can be achieved by the intensity correlation criterion. However, the position of the cylinder is most closely indicated by the point of maximum intensity on each arc, with the remainder of the arc feature being an artefact arising due to the limited azimuthal resolution of the real image. Co-registration was also conducted using an alternative entropy-based mutual information criterion but without significantly different results. Closer inspection of Figure 18 shows that there is not a single rigid transformation that will align all arc features; the images are not sufficiently similar to enable meaningful co-registration.

A quantitative study was then carried out over a number of ping pairs to assess the consistency of co-registration outcomes. For six adjacent ping pairs, images were co-registered, and then divided into quarters with each corresponding pair of quarters individually co-registered. Ideally this would have shown consistent inferred displacements across image fragments but instead there is significant variability. Alternatively, constraining yaw and surge to values derived from inertial navigation and the Doppler velocity log did not result in significant improvement. From this it is concluded that there is an insufficient quantity of similar information present in the paired imagery.

5 CONCLUSIONS

DPIA has been successfully implemented but was not found to be any more successful than DPCA when applied to a challenging subset of trials data. The reasons for this outcome are considered to be the low azimuthal resolution of the real-aperture images and insufficient similarity between successive images. While DPIA may yet offer improved robustness in other scenarios/hardware

configurations, any such improvement has not been sufficient to enable the trials data in question to be postprocessed into SAS imagery.

The most obvious route to facilitating DPIA (or DPCA) would be to improve the quality of the acquired data, in this case by exploiting the full capability of MUSCLE (such as improved vertical directivity/sensitivity, and use of additional array elements within a multipath mitigation scheme). In the general case, in the absence of such capability, azimuthal resolution of real aperture imagery could be improved by the use of higher frequency sonar (with consequent drawbacks relating to signal power dissipation, computational burden and more demanding micronavigation requirements), or via longer sonar arrays with more elements (which may not be compatible with existing commercial off-the-shelf AUV form factors). These improvements would contend with the root cause of the difficulty in processing the Biodola Bay data, i.e. limited signal-to-noise ratio. If the improvements enabled DPIA to function effectively, it could be possible to significantly increase the area mapping rate of AUV SAS platforms beyond that possible with DPCA.

If the opportunity arose for further investigation, the real-aperture images could be modified to incorporate a feature detection or non-linear rescaling stage prior to co-registration, and a numerical study could be conducted to map out the hardware parameter space over which DPIA would be likely to be effective given echo returns with a particular signal-to-noise ratio.

6 FUNDING AND ACKNOWLEDGEMENTS

The authors gratefully acknowledge financial support from the Centre for Defence Enterprise / Dstl, and also thank CMRE for the loan of the trials data and supporting with its interpretation.

7 REFERENCES

1. M. Pinto, A Bellettini, Shallow water synthetic aperture sonar: an enabling technology for NATO MCM forces, NATO Undersea Research Centre NURC-PR-2007-010, La Spezia, Italy, 2007; originally published in Undersea Defence Technology Europe, Naples, Italy (5-7 June 2007).
2. A. Bellettini and M. A. Pinto, Accuracy of Synthetic Aperture Sonar Micronavigation using a Displaced Phase Centre Antenna: Theory and Experimental Validation, SACLANT Undersea Research Centre Report SR-355 (February 2002).
3. M. Pinto, Design of Synthetic Aperture Sonar Systems for High-Resolution Seabed Imaging, NURC-PR-2006-029 (October 2006).
4. M. Pinto, A. Bellettini, and R. Hollett, L. Wang, MUSCLE: A Minehunting UUV With Synthetic Aperture Sonar Capability for Littoral Operations, Proceedings of the International Conference "Underwater Acoustic Measurements: Technologies & Results", Heraklion (June 2005).
5. B. Evans, F. Baralli, A. Bellettini, E. Bovio, E. Coiras, G. Davies, J. Groen, V. Myers, and M. Pinto, AUV Technology for Shallow Water MCM Reconnaisance, NATO Undersea Research Centre Report NURC-PR-2007-008 (October 2007).
6. F. Baralli, M. Couillard, J. Ortiz, and D. G. Caldwell, GPU-Based Real-time Synthetic Aperture Sonar Processing On-board Autonomous Underwater Vehicles, OCEANS 2013, Bergen (10-14 June 2013).
7. A. Belletini, M. Pinto, P. Munk, V. Myers, A New Synthetic Aperture Sonar Design with Multipath Mitigation, Int. Conf. Acoustics, Kyoto, Japan (April 2004) (invited).
8. M. Zampolli, MARES 2008 Post-Cruise Briefing (presentation slides), NURC (16 April 2008).
9. P. T. Gough and M. A. Miller, Displaced Ping Imaging Autofocus for a Multi-Hydrophone SAS, IEE Proceedings, Radar Sonar and Navigation Volume 151 Issue 3 (12 June 2004).
10. P. T. Gough and D. W. Hawkins, Unified Framework for Modern Synthetic Aperture Imaging Algorithms, International Journal of Imaging Systems and Technology, Volume 8, Issue 4, pp 343-358 (1997).